J. Fluid Mech. (1994), *vol.* 259, *pp.* 79–106

Experimental study of dipolar vortices on a topographic β-plane

By O. U. VELASCO FUENTES AND G. J. F. VAN HEIJST

Laboratory of Fluid Dynamics and Heat Transfer, Faculty of Physics, Eindhoven University of Technology, P.O. Box 513, 5600 MB Eindhoven, The Netherlands

(Received 22 December 1992 and in revised form 14 June 1993)

The behaviour of dipolar vortices in a rotating fluid with a sloping bottom (simulating the variation of the Coriolis parameter on the Earth, with the direction of steepest bottom slope corresponding with the northern direction) has been investigated in the laboratory. Dipoles were generated by moving a vertical cylinder through the fluid. Dye photographs provided qualitative information, whereas quantitative information about the evolving flow field was obtained by streak photography. Dipoles initially directed under a certain angle relative to the west–east axis showed meandering or cycloid-like trajectories. Some asymmetries between east-travelling dipoles (ETD's) and west-travelling dipoles (WTD's) were observed. ETD's are stable in the trajectory sense: a small deviation from zonal motion results in small oscillations around the equilibrium latitude. WTD's are unstable: small initial deviations produce large displacements in northern or southern directions. This asymmetry arises because the vorticity of a dipole moving westward is anticorrelated with the ambient vorticity, while the vorticities are correlated when the dipole moves eastward. ETD's increase in size and eventually split into two independent monopoles, the rate of growth depending on the gradient of planetary vorticity. WTD's are initially more compact but owing to the large displacements in the meridional direction strong asymmetries in the circulation of the two halves are produced, resulting in a large deformation of the weaker part. The experimental observations show good qualitative agreement with analytical and numerical results obtained using a modulated point-vortex model.

1. Introduction

Two-dimensional flows are characterized by the emergence of coherent vortices (see e.g. McWilliams 1984). Among these, the monopolar vortex is the most frequently occurring vortex type. The dipole, consisting of two closely packed counter-rotating vortices, is another notable member of the family of coherent vortex structures. Dipolar vortices have been observed in laboratory experiments under a variety of circumstances. For example, they may appear as the organized two-dimensional product of a pulsed, turbulent jet, in both stratified and rotating fluids (van Heijst & Flór 1989; Flierl, Stern & Whitehead 1983); in the wake of a cylinder moving through a soap film (Couder & Basdevant 1986); and in magnetohydrodynamic flows (Nguyen Duc & Sommeria 1988). High-resolution numerical simulations of two-dimensional turbulence also show the emergence of dipolar vortices (Legras, Santangelo & Benzi 1988). In nature, dipoles have been observed in the form of 'mushroom-like' currents in the ocean (Fedorov & Ginsburg 1989) and as 'blocking' events in the atmosphere (Haines & Marshall 1987).

The dipolar vortex has two remarkable properties: it possesses a separatrix and it

has a non-zero linear momentum. This means that the dipole provides an efficient mechanism for the transport of mass and momentum over large distances. In particular, oceanic dipolar vortices are believed to play an important role in the transport of scalar properties such as heat, salt, nutrients and other biochemical components.

The two-dimensional character of large-scale motions in the oceans and in the atmosphere is due to both rotation, which makes the fluid move in (locally) horizontal planes, and geometry, since the ratio between horizontal and vertical scales is of $O(10^3)$. The dynamics of geophysical flows is further fundamentally influenced by the gradient of the Coriolis parameter in the latitudinal direction, usually referred to as the β-effect.

The simplest model that includes these effects is the so-called equivalent barotropic vorticity equation, which expresses the conservation of potential vorticity in a homogeneous, incompressible two-dimensional flow on a rotating sphere (see Pedlosky 1979). In the context of plasma physics, this equation is known as Hasegawa–Mima equation, where a density gradient plays the same role as the gradient of the Coriolis force (see e.g. Makino, Kamimura & Taniuti 1981). In the sequel of this paper the equation will be used in the limit of infinite radius of deformation, but the results presented here have relevance to both geophysical flows and plasmas.

The equivalent barotropic equation has a number of dipolar solutions, which are also known as modons. One common characteristic of modons is that, besides having a separatrix, they are either stationary or they translate perpendicularly to the gradient of ambient vorticity. The travelling modons thus provide a mechanism for transport along the isolines of ambient vorticity. An important question concerns the existence of similar structures that propagate transversally to those isolines.

Although a modon is not an exact solution when its symmetry line is not parallel to isolines of ambient vorticity, Makino *et al.* (1981) used 'tilted' modons as initial conditions for numerical simulations. They found that the modons survived as coherent structures, moving along meandering trajectories in an eastward direction or along cycloid-like paths in a westward direction, depending on the tilting angle. Using a perturbation technique, Nycander & Isichenko (1990) also found these two regimes as well as the mode in between, in which the dipole performs a periodic looping excursion without any net displacement. They also calculated the decay rate based on vorticity generation in the wake of the dipole. The decay was found to be insignificant on the timescales of an oscillation of the dipole's motion.

Another approach to the problem has been the use of a couple of point vortices of equal but opposite strengths and allowing variations in relative circulation to preserve potential vorticity during the evolution. Kawano & Yamagata (1977) first found the three 'regimes' in the motion of the couples: (i) eastward meandering; (ii) westward cycloid-like trajectories; and (iii) the 'non-propagating' mode, in which the couple moves along an 8-shaped curve fixed in space. Zabusky & McWilliams (1982) presented calculations of a point-vortex couple and a dipole represented by two pairs of point-vortices. These point-vortex calculations showed good agreement with numerical simulations of a modon solution, at least for the first oscillation. More recently, Kono & Horton (1991) presented an exact solution for the motion of the point-vortex dipole as well as numerical results of interactions of point-vortex couples in an inhomogeneous medium. Hobson (1991) studied the problem in phase-space terms and found that the dipole moving to the east has a stable trajectory, while that of a westward-travelling dipole is unstable. Makino *et al.* (1981) found the same behaviour in their numerical simulations of modons. However, they did not use the

terms stable or unstable trajectories, as pointed out by Nycander (1992), who refers to it as 'tilt' instability.

In a combined analytical/numerical approach Swaters & Flierl (1989) examined the Ekman dissipation of an east-travelling dipole. They found that the distance between the vorticity extrema grows linearly in time, while the velocity of the structure decreases monotonically.

A gradient of the ambient vorticity can also be caused by variations of the depth of the rotating fluid. When the variations are linear and small, the gradient of ambient vorticity is approximately the same as that produced by the variation of the Coriolis parameter; this effect is sometimes referred to as the 'topographic β-effect'. Carnevale *et al.* (1988) numerically studied the motion of dipoles over hills and ridges and found that under strong topographies the dipole broke apart, the cyclonic half moving uphill and the anticyclonic one downhill. The evolution of the independent halves after the splitting corresponds with the general behaviour of barotropic monopolar vortices on a β-plane, namely: cyclones move to the (local) northwest and anticyclones move to the (local) southwest. The problem of a single monopole on a β-plane has received considerable attention in the last decades, both in theoretical studies (Adem 1956), in numerical and laboratory experiments (Carnevale, Kloosterziel & van Heijst 1991), and in observational studies (see Robinson 1983).

Experimental studies on dipolar vortices have concentrated mainly on situations without a gradient of ambient vorticity (β-effect absent). Nguyen Duc & Sommeria (1988) studied vortex couples in a thin layer of mercury, the flow being constrained to be two-dimensional by an external magnetic field. They obtained steadily translating dipoles; the symmetric dipoles (with zero net circulation) were seen to translate along straight paths, whereas the trajectories of asymmetric dipoles (with non-zero circulation) were found to be circular. Nguyen Duc & Sommeria also determined the relationship between the vorticity ω and the stream function ψ of the laboratory dipoles, and they found both linear and nonlinear (sinh-like) relations. Flór & van Heijst (1993) compared the Lamb model, which assumes a linear ω–ψ relation in the interior of the dipole, with their experimental observations of dipoles in a stratified fluid. The experimental results (vorticity distribution, dipole size and translation speed) show very good agreement with the Lamb dipole, both for dipoles with a linear ω–ψ relation and for dipoles with a nonlinear relation. In their rotating-fluid experiments, Flierl *et al.* (1983) studied dipolar vortices that contained non-zero circulation, and accordingly travelled along a circular path. By taking into account the net circulation they obtained a modified Lamb dipole solution, which was found to agree well with their experimental results.

The results to be discussed in the present paper concern the behaviour of dipolar vortices when a weak gradient of ambient vorticity is present in the system. The following section reviews the main results of the modulated point-vortex dipoles and shows that the meandering of the trajectory also arises for slightly asymmetric couples. After a brief description of the experimental technique in §3, experimental observations of dipole trajectories for different initial directions, and the corresponding evolution of velocity and size, are presented in §4. Flow measurements during one oscillation of the dipole are also presented. A comparison between west-travelling dipoles (WTD's) and east-travelling dipoles (ETD's) is made in §5, on the basis of both experimental observations and numerical results obtained with a vortex-in-cell method. The behaviour of an ETD for different values of β is discussed in §6. Finally, in §7 we discuss the results and draw some general conclusions.

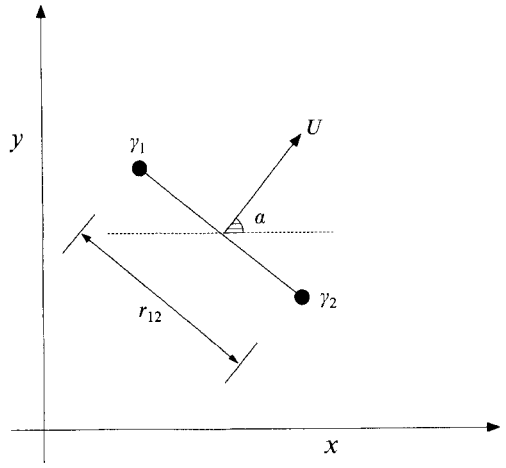

FIGURE 1. Schematic representation of the point-vortex model of a dipole.

2. The modulated point-vortex model

For completeness, first the motion of a symmetric pair of point vortices on a β-plane is reviewed. The vortices' circulations are modulated so that potential vorticity is conserved. The results are then extended to non-symmetric pairs. The case of a symmetric pair and a finite deformation radius can be found in the references mentioned in the previous section.

In the absence of background vorticity the evolution of a group of N point vortices is governed by a system of $2N$ ordinary differential equations (e.g. Batchelor 1967):

$$\frac{\mathrm{d}x_i}{\mathrm{d}t} = -\frac{1}{2\pi}\sum_{\substack{j=1\\ j\neq i}}^{N} \gamma_j \frac{y_i - y_j}{r_{ij}^2}, \quad \frac{\mathrm{d}y_i}{\mathrm{d}t} = \frac{1}{2\pi}\sum_{\substack{j=1\\ j\neq i}}^{N} \gamma_j \frac{x_i - x_j}{r_{ij}^2}, \tag{2.1}$$

where (x_i, y_i) is the position of point vortex i with circulation γ_i, and r_{ij} is the distance between vortices i and j.

Large-scale motions on a rotating sphere (the Earth) are fundamentally affected by the latitudinal variation of the Coriolis parameter f, which is defined as $f = 2\Omega \sin\phi$, with Ω the Earth's angular speed and ϕ the geographic latitude. For motions occurring on scales smaller than a few degrees of latitude the Coriolis parameter can be approximated as a constant (local) value plus a linear variation in the meridional direction, i.e. $f = f_0 + \beta y$, where $f_0 = 2\Omega \sin\phi_0$ and $\beta = 2\Omega \cos\phi_0 / R$, with R the Earth's radius. This approximation is known as the β-plane model.

Conservation of potential vorticity implies that the relative vorticity ω of a vortex tube moving in the meridional direction changes, as expressed by the following equation:

$$\frac{\mathrm{D}}{\mathrm{D}t}(\omega + \beta y) = 0, \tag{2.2}$$

where $\mathrm{D}/\mathrm{D}t = \partial/\partial t + u\partial/\partial x + v\partial/\partial y$ is the material derivative, and u and v are the velocities in the east (x) and north (y) directions, respectively.

Although a potential point vortex is not a solution of (2.2) for the case $\beta \neq 0$, some insight into the β-plane dynamics can be gained by solving (2.1) with the circulations being modulated according to the principle of conservation of potential vorticity. For that purpose it is necessary to assign a certain area to the 'point' vortex: under the

assumption that a point vortex represents a small patch of vorticity, the circulation equals the (uniform) vorticity $\bar{\omega}$ multiplied by the area of the patch. If πL^2 is the area associated with the point vortex, its circulation is then given by $\gamma = \bar{\omega}\pi L^2$.

Using (2.2) and conservation of mass one obtains

$$\gamma_i = \gamma_{0i} + \pi L^2 \beta (y_{0i} - y_i). \tag{2.3}$$

In this expression y_{0i} represents the initial latitude, at which the vortex has strength γ_{0i}.

For a system of just two point vortices the distance r between them is a constant of motion. This fact makes it possible to describe the evolution of the pair with the position of the middle point and the direction of motion (figure 1). Substituting the new variables

$$\eta = \frac{x_1 + x_2}{2}, \quad \xi = \frac{y_1 + y_2}{2}, \quad \alpha = \arctan\left[-\frac{x_2 - x_1}{y_2 - y_1}\right] \tag{2.4}$$

in (2.1), one obtains

$$\left.\begin{aligned} &\frac{\mathrm{d}\eta}{\mathrm{d}t} = \frac{1}{4\pi r}(\gamma_1 - \gamma_2)\cos\alpha, \quad \frac{\mathrm{d}\xi}{\mathrm{d}t} = \frac{1}{4\pi r}(\gamma_1 - \gamma_2)\sin\alpha, \\ &\frac{\mathrm{d}\alpha}{\mathrm{d}t} = \frac{1}{2\pi r^2}(\gamma_1 + \gamma_2), \end{aligned}\right\} \tag{2.5}$$

where the third expression is a general equation for the angular velocity of a pair of point vortices.

For the case of an initially symmetric dipole $\gamma_1 = -\gamma_2 = \gamma_0$, one obtains the following system of ordinary differential equations governing the motion of the pair:

$$\frac{\mathrm{d}\eta}{\mathrm{d}t} = U\cos\alpha; \quad \frac{\mathrm{d}\xi}{\mathrm{d}t} = U\sin\alpha; \quad \frac{\mathrm{d}\alpha}{\mathrm{d}t} = -\frac{\beta L^2}{r^2}(\xi - \xi_0), \tag{2.6a–c}$$

where

$$U = \frac{\gamma_0}{2\pi r}\left[1 - \frac{\beta\pi L^2 r}{2\gamma_0}(\cos\alpha - \cos\alpha_0)\right].$$

For a relatively weak β-effect with respect to the vortex circulation ($\beta r L^2/\gamma_0 \ll 1$) the translation velocity of the dipole can be approximated by $U \approx U_0 \equiv \gamma_0/2\pi r$.

Note that (2.6a) is a subsidiary relation and the whole evolution is determined by (2.6b) and (2.6c), which can be combined to yield a single equation for α:

$$\frac{\mathrm{d}^2\alpha}{\mathrm{d}t^2} + \frac{L^2}{r^2}\beta U_0 \sin\alpha = 0. \tag{2.7}$$

The solution should satisfy the initial conditions $\alpha(0) = \alpha_0$, which is the tilting angle, and $\alpha'(0) = 0$, since the couple is initially symmetric. This is the nonlinear simple pendulum equation. A few results can be drawn immediately from its linearized version: for small values of α_0 the oscillations have a constant frequency $(L/r)(\beta U_0)^{\frac{1}{2}}$ and the wavelength λ and the amplitude A of the oscillations are given by

$$\lambda = \frac{r}{L}\left(1 - \frac{\alpha_0^2}{4}\right)2\pi\left(\frac{U_0}{\beta}\right)^{\frac{1}{2}}; \quad A = \frac{r}{L}\alpha_0\left(\frac{U_0}{\beta}\right)^{\frac{1}{2}}.$$

Proceeding with the analogy between the vortex pair and the pendulum, an ETD ($\alpha_0 = 0$) clearly has a stable trajectory: when a small perturbation is imposed, small oscillations around the equilibrium latitude arise. On the other hand, a WTD ($\alpha_0 = \pi$)

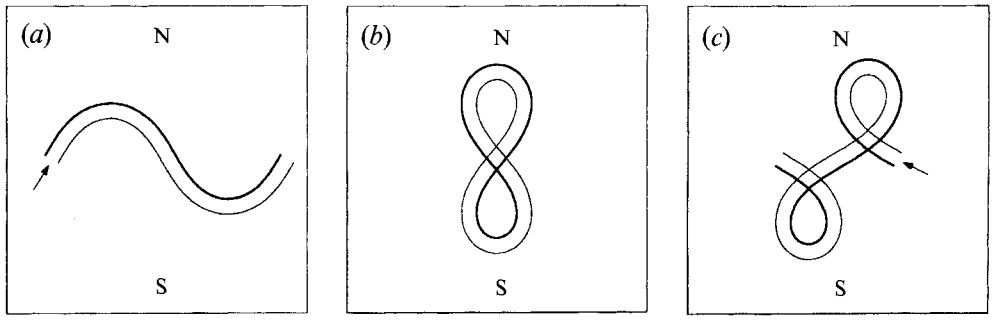

FIGURE 2. Trajectory modes of a modulated point-vortex dipole on a β-plane: (*a*) the meandering mode, with eastward drift; (*b*) the 'non-propagating' mode, with the dipole moving along an 8-shaped path fixed in space, and (*c*) the cycloid mode, with westward drift. The dipole was initially symmetric and moved in the direction indicated by the arrow. The thick line represents the path of the positive vortex, the thin line the path of the negative vortex. The upper and lower parts of the plots correspond to north and south, respectively.

is unstable in the trajectory sense (see also Hobson 1991). This instability is also present in continuous modons and has important consequences for the stability of the structure itself (Makino *et al.* 1981; Nycander 1992). The effect on laboratory modons will be discussed in §4.1.

Figure 2 shows numerical integrations of (2.1) and (2.3) with the corresponding regimes: (*a*) wave-like trajectory, (*b*) 8-shaped trajectory and (*c*) cycloid-like trajectory. These regimes were originally described by Kawano & Yamagata (1977), although their paper seems to have escaped the attention of most of the investigators working in this field (most likely because the paper is written in Japanese).

The condition of initial symmetry of the two point vortices can be relaxed ($\gamma_2/\gamma_1 = a \neq -1$). An approximate equation with the same form as (2.7) can again be obtained, but in this case $U \approx U_0 \equiv \frac{1}{2}(1-a)\gamma_0/2\pi r$ and the initial condition for the angular velocity changes to $\alpha'(0) = \Omega_0 \equiv (1+a)\gamma_0/2\pi r^2$, owing to the asymmetry of the initial dipole. The same oscillatory behaviour arises for $\Omega_0^2 < (L^2/r^2)\beta U(\cos\alpha_0 + 1)$. However, in this case the equilibrium latitude is not the latitude of the initial position. The dipole meanders around a line located to the north of the initial position if the positive vortex is initially stronger (figure 3*b*). Likewise, if the negative vortex is stronger the equilibrium latitude is located to the south of the initial position (figure 3*a*). If $\Omega_0^2 > (L^2/r^2)\beta U(\cos\alpha_0 + 1)$ the dipole remains always asymmetric and rotates around a point that moves westward (figure 3*c*, *d*).

It was brought to our attention by Professor Vyacheslav V. Meleshko that the equations of motion discussed here are analogous to those describing the equilibrium shape of a thin elastic rod bent by a combination of forces and force couples applied at its ends (Love 1944). The path of an initially symmetric dipole is analogous to the shape of the rod when only forces are applied at its ends. On the other hand, an asymmetric dipole moves along a trajectory whose shape is similar to that of the bent rod when both forces and couples are applied at its ends (see figures 48 to 56 in Love 1944).

It is appropriate to make some comments on the two lengthscales r and L present in the problem, being the distance between the two point vortices and the radius of the area associated with each 'point vortex', respectively. It is stressed that while being arbitrary, L must be much smaller than r, otherwise the discrete representation of the vortex patch is not accurate. Also, L must be finite, otherwise the modulation mechanism does not work.

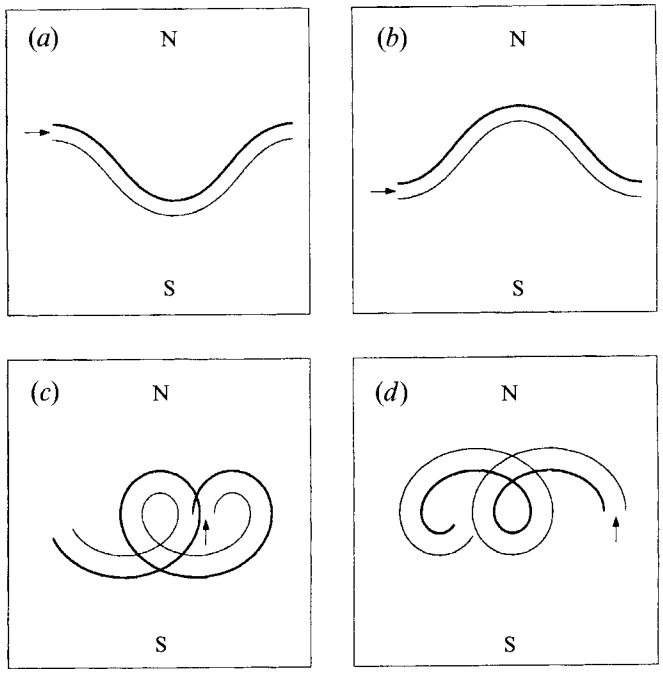

FIGURE 3. Trajectories of initially non-symmetric point-vortex dipoles on a β-plane. (*a*) Slightly negative net circulation causes meandering around a line southward of the equilibrium latitude, (*b*) slightly positive net circulation causes meandering around a line northward of the equilibrium latitude, (*c*) strong negative circulation causes anticyclonic librations around a point that drifts to the west, and (*d*) strong positive net circulation produces cyclonic librations and westward drift.

The regimes obtained with this simple model do not depend on the special condition of having an initially symmetric dipole. However, several effects are neglected in the model: (i) it is assumed that each 'point' vortex has a finite core, but its deformations are not taken into account; and most importantly, (ii) the effect of relative vorticity being generated by advection of ambient fluid has totally been neglected in the model. Naturally, the question arises of whether dipolar vortices in real flows would show phenomena similar to those described above. In order to provide an answer to that question, we have carried out a study of dipolar vortices in the well-controlled laboratory environment.

3. Experimental arrangement

3.1. *Laboratory simulation of a β-plane*

It is well known that a smoothly varying bottom topography in a rotating system produces an equivalent result to the variation of the Coriolis parameter for a rotating sphere, usually referred to as the topographic β-effect. If we consider the shallow-water equations in a rotating system (Laplace's tidal equations), the following conservation relation can be obtained:

$$\frac{\mathrm{D}}{\mathrm{D}t}\left[\frac{\omega+f_0}{h(x,y)}\right]=0, \tag{3.1}$$

where ω is the relative vorticity, $f_0 = 2\Omega$ is twice the constant rate of rotation and $h(x,y)$ is the depth of the fluid.

Let h have a small linear variation in some direction, say y, so that the fluid depth as a function of position is given by $h(y) = h_0(1-sy)$, with s a small parameter. Substituting this expression in (3.1) and expanding the result in a Taylor series one obtains

$$\frac{\mathrm{D}}{\mathrm{D}t}[\omega + sf_0 y] = 0, \tag{3.2}$$

where a small Rossby number ($\omega/f_0 \ll 1$) is assumed. This equation is equivalent to (2.2), showing that to this order of approximation the dynamics of a rotating fluid in a container with a linearly varying bottom topography is equivalent to that of a fluid on a β-plane. Obviously, the equivalent β-value is $\beta = sf_0$.

3.2. *Apparatus*

The experiments were carried out in a rectangular tank of horizontal dimensions 100×150 cm and 30 cm depth mounted on a rotating table. The angular speed of the system could be varied continuously and was in most experiments taken as $\Omega = 0.56\ \mathrm{s}^{-1}$, so that the Coriolis parameter $f = 1.12\ \mathrm{s}^{-1}$. The working depth of the fluid was varied from 15 to 20 cm, and a false bottom was raised 4–8 cm along one of the long sides to provide the topographic β-effect. With these parameter settings the equivalent value of β measured approximately $0.25\ \mathrm{m}^{-1}\ \mathrm{s}^{-1}$. This choice of parameter values was made in order to achieve two effects: (i) a dynamically relevant gradient of background vorticity without affecting the two-dimensionality of the motion; and (ii) a column of fluid long enough for the effect of the bottom Ekman layers to be negligible on the timescale of the experiment, e.g. the time required for the dipole to cross the tank (in the absence of bottom topography typically 10–20 rotation periods). Exact parameter values of particular experiments are given where appropriate.

3.3. *Dipole generation*

The experiment was started by filling the tank to the desired height. Then the fluid was spun-up to an angular velocity of $0.56\ \mathrm{s}^{-1}$, a process that takes typically a few minutes. In order to avoid even very weak background flows, however, in all experiments the fluid was allowed to spin-up for approximately 30 minutes. A columnar dipole vortex was generated by slowly moving a small, bottomless cylinder of 8 cm diameter in a straight line relative to the rotating tank, while gradually lifting it (figure 4). By moving the cylinder very slowly (10–$15\ \mathrm{cm\ s}^{-1}$) and keeping its axis parallel to the axis of rotation, one guarantees that the forcing is almost two-dimensional. The vorticity generated by the motion of the cylinder accumulates in a dipolar structure in the wake of the cylinder. This dipolar flow is confined in a vertically aligned Taylor column, a feature well-known in rotating fluids. After typically 1–2 rotation periods the organization of the vortex flow is completed, and the mature, fairly symmetric dipole travels through the fluid along an almost straight line.

The radius of deformation $R_d = (gh)^{\frac{1}{2}}/f$ varied with the experimental configuration from 1 to 1.25 m. These values are much greater than the typical size of the dipole (0.1 m). A Rossby number for the generation process is defined as $Ro = U/2\Omega R$, with Ω the rotation rate of the system and U and R the velocity and radius of the cylinder, respectively. According to the parameters given above this Rossby number is of order 2–3. A Rossby number for the resultant dipolar structure is defined with U as the maximal velocity and R as the distance between the points of the extremal values of vorticity. This Rossby number is measured to be of order 0.1–0.2 when the dipole reaches a mature state, in all the experiments discussed in this paper.

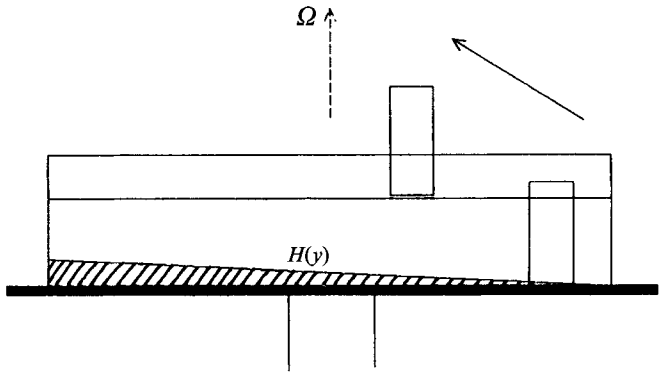

FIGURE 4. Schematic view of the experimental arrangement. The tank rotates with a constant angular velocity Ω, and the β-effect is provided by a sloping bottom (with shallow being equivalent to 'north'). Dipoles are generated by dragging a small bottomless cylinder (8 cm in diameter) through the fluid while lifting it as indicated in the figure. The typical speed of the cylinder is 0.15 m s^{-1}.

The generation technique described above proved to be superior to the injection of a turbulent jet, since in that case the forcing is essentially three-dimensional. The jet is deflected by the Coriolis force and tends to move anticyclonically in a circular trajectory. One of the two-dimensional products of this process is an asymmetric dipole (Flierl *et al.* 1983).

3.4. *Flow visualization*

In a first series of experiments dye (fluorescine or terasil blue) was added to the fluid within the small cylinder before dragging it through the ambient fluid in the rotating tank. These experiments provided important qualitative information about the adjustment process and allowed the two-dimensionality of the motion to be verified. Indeed, the dipole moved as an almost circular cylinder (Taylor column) through the ambient fluid, carrying most of the dye with it. In each experiment the flow was recorded photographically (photographs were taken at intervals of typically 5–15 s) by a camera mounted in the rotating frame about 150 cm above the free surface of the fluid.

Dye experiments were done mainly to determine the trajectory of the dipole as a function of the initial direction, and to estimate the dipole's size and velocity during its evolution. This information was obtained by projecting the negative film on a screen and plotting the centres of the dye patterns. Each centre is determined from the spiral structure within each half of the dipole and from the shape of the whole vortex. The distance between the centres is considered as a measure of the size of the dipole; hereafter this distance will be referred to as the 'size' of the dipole. From a series of positions the linear displacement as function of time can be obtained, providing the integrated velocity as a function of time.

3.5. *Flow measurements*

Flow measurements were made from photographic streaks of small (1 mm diameter) paper particles floating on the free surface, and sprinkled randomly all over the tank before a dipole was generated. In such experiments, pictures were taken every 15 s and the exposure time was varied from 1 s at the beginning of an experiment to 3–4 s at later stages. The typical duration of an experiment was 20–25 rotation periods.

The velocity field is measured from the lengths and orientations of particle streaks, which are approximated by straight line segments. With the help of a digitization table

the coordinates of the start and end points of the streaks are loaded into a personal computer. The distance between these points divided by the exposure time gives the mean local velocity of the fluid. Then the velocity field is interpolated onto a regular grid of 30×30 points by using cubic splines (for details of this technique, see Nguyen Duc & Sommeria 1988).

The analytic functions that give the values of the velocity components u and v on each grid point can then be differentiated to obtain the vertical component ω of the vorticity in the grid points:

$$\omega = \frac{\partial v}{\partial x} - \frac{\partial u}{\partial y}. \tag{3.3}$$

The stream function ψ is computed from the vorticity field by numerically solving the Poisson equation:

$$\nabla^2 \psi = -\omega. \tag{3.4}$$

The boundary conditions for ψ are obtained (within an arbitrary constant) from the line integral of the normal velocity on the edge.

The stream function ψ' in a frame of reference moving with the couple can be calculated by simple transformation:

$$\psi' = \psi - U_x y + U_y x \quad \text{or} \quad \psi' = \psi + \tfrac{1}{2}\Omega' R^2, \tag{3.5}$$

with U_x and U_y being the components of the translation velocity, Ω' the angular velocity of the dipole and R the distance to the dipole's centre of rotation. In the case of pure linear translation the vorticity remains unchanged, whereas a constant value ($2\Omega'$) must be added in the case of a rotational motion.

The parameters needed to correct for rotation or linear translation are obtained from photographs taken before and after the one being analysed. From this sequence of pictures, one can estimate the magnitude and direction of the velocity, or the angular speed and the apparent centre of rotation. Throughout the following sections only the corrected stream function ψ' will be used, but the prime will be omitted to simplify notation.

4. A meandering dipole

4.1. *Qualitative observations*

The basic mechanism that determines the trajectory of a dipole on a β-plane has already been explained by Makino *et al.* (1981). In order to clarify some of the laboratory observations to be discussed later, the argument will be repeated here in terms of fluid-depth variations.

The dipolar vortex was generated by moving the cylinder along a straight line in a 'northern' direction, i.e. into shallower parts of the tank. Once the dipole has reached a mature state (figure 5*a*), it tends to move in a straight line to the northeast, where the fluid is shallower. Owing to the background rotation the two dipole halves experience asymmetric effects, as can be understood from (3.1): the cyclonic vortex ($\omega > 0$) becomes weaker while the anticyclonic one ($\omega < 0$) becomes stronger, resulting in a trajectory curved in a clockwise sense. The vertical squeezing also causes the dipole to widen, so that the vorticity extrema move slightly apart and the translation velocity decreases. The dipole reaches a maximum size and a maximum circulation asymmetry at its northernmost position (figure 5*b*). The clockwise rotation brings the dipole southwards, and the asymmetry gradually diminishes. The dipole recovers its zero net

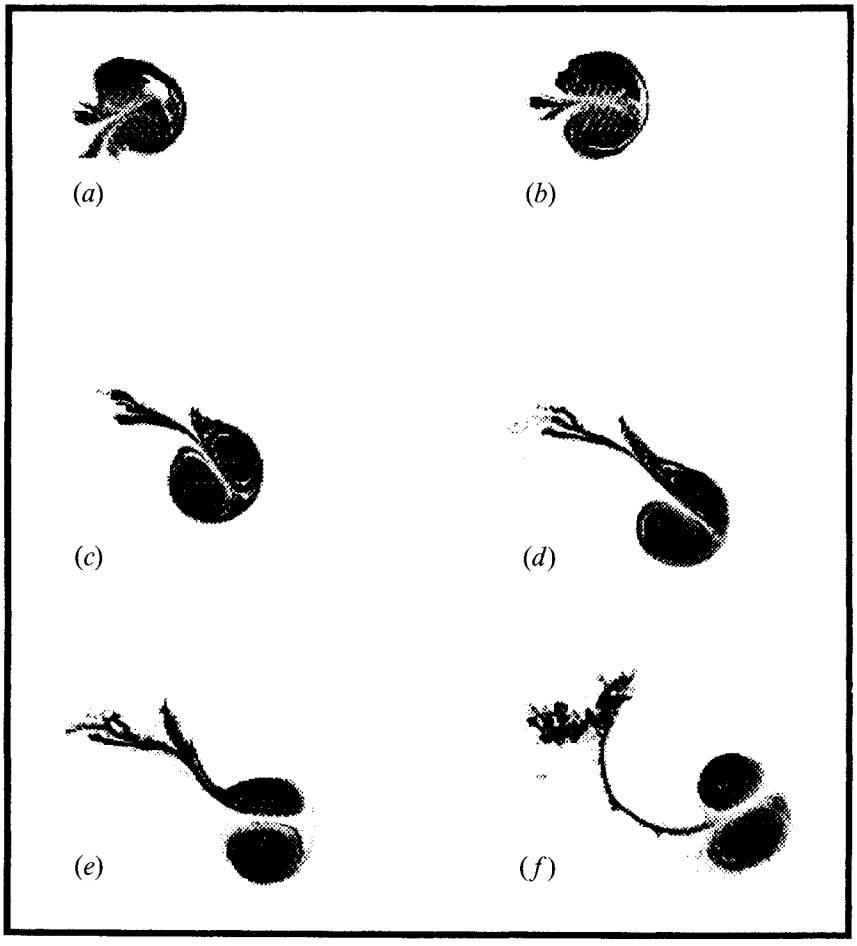

FIGURE 5. Sequence of plan-view photographs showing the meandering of a dipolar vortex on a (topographic) β-plane. The dipole was created as indicated in figure 4 and it travelled initially towards shallower fluid (top of the pictures). The images were taken at times (*a*) $t = 3.1T$, (*b*) $6.7T$, (*c*) $8.8T$, (*d*) $12.1T$, (*e*) $15.3T$ and (*f*) $29.7T$ after withdrawing the cylinder, with $T = 11.1$ s the rotation period of the turntable. Experimental parameters: $f = 1.13$ s^{-1}, $h_0 = 0.18$ m, $s = 0.22$ m^{-1}, $\beta = 0.25$ m^{-1} s^{-1}.

circulation when it crosses the equilibrium line, where the height of the fluid column is equal to its initial value (figure 5*c*). Because of its own momentum the dipole moves further into deeper regions ('south') so that the column of fluid is stretched further. Owing to this stretching, the cyclonic half ($\omega > 0$) becomes stronger while the strength of the anticyclonic part of the dipole decreases in magnitude. As a result the dipole's trajectory curves in an anticlockwise sense (figure 5*d*). The stretching also causes the vorticity extrema to get closer, and as a consequence the translation speed of the dipole increases at this stage. After reaching its southernmost position (figure 5*e*), the dipole moves back to its equilibrium depth (figure 5*f*), and the meandering process continues.

Experimentally, we have not been able to observe more than one cycle of the oscillatory path, because the dipole either reached the wall after one meandering or it was observed to split into two monopolar vortices. The latter feature will be discussed in more detail in §6.

4.2. *Flow measurements*

Results equivalent to those described in the previous section are obtained when the dipole moves southward initially, as can be seen from the flow evolution (figures 6–9). When it reaches a mature state at time $t = 1.77T$, with T the rotation period of the table ($T = 11.3$ s), the dipole moves in an approximate southeast direction. The cyclonic half is stronger, resulting in an anticlockwise deflection of the dipole's trajectory. The density of the vorticity contours in figure 6*a* shows a clear asymmetry between the two dipole halves. The streamline pattern $\psi = \text{const}$ (see figure 6*b*) shows the same asymmetry; the centre of the rotational dipole motion at this stage is also visible in the upper right corner of the figure.

At $t = 4.42T$ the dipole reaches its southernmost position; therefore a maximum asymmetry is observed in the contours of vorticity (figure 7*a*) and a decrease of size with respect to the previous stage (cf figure 6*a*). The same effects can be observed in the streamline pattern (figure 7*b*). Also, the curvature of the dipole trajectory has increased at this stage, as can be observed from the centre of rotation, which has moved closer to the dipole.

As the dipole returns to its equilibrium depth (at $t = 7.96T$) the asymmetry is reduced, as can be observed from the vorticity distribution (figure 8*a*). The dipole size increases and the centre of rotation moves farther away (figure 8*b*). However, the dipole still has positive circulation and its path is curved in an anticlockwise sense.

Finally, at $t = 15.93T$ the dipole reaches its northernmost position, as shown in figure 9. The clockwise rotation and the vorticity contours reveal that the dipole has acquired a negative net circulation (figure 9*a*). The centre of rotation is now located to the south (figure 9*b*). The low density of contour lines in both the vorticity and the stream function plots indicates the decay of the dipole, which is most likely produced by two mechanisms associated with the topographic β-effect. First, the generation of relative vorticity in the wake of the dipole, and second, the entrainment and detrainment of ambient fluid (or 'breathing', Nycander & Isichenko 1990). The observed evolution of similar dipoles on the f-plane shows that other decay mechanisms like horizontal diffusion or spin-down induced by the Ekman layers are insignificant on this timescale (approximately 15 rotation periods).

The evolution of the total relative circulation within the dipole illustrates a few important characteristics. The circulation is obtained by a (discrete) surface integral of the vorticity values. The ratio $\epsilon = |(\gamma^+/\gamma^-)|$, with γ^+ the positive circulation and γ^- the negative circulation in the dipole, changes as the position of the dipole moves in a meridional direction. At $t = 1.77T$ (figure 6) the ratio ϵ measures 1.23, showing that there is an excess of positive vorticity and therefore an anticlockwise rotation. In the southernmost position (figure 7) the circulation reaches its most positive value and $\epsilon = 1.488$. Afterwards the asymmetry starts to decrease; at $t = 7.96T$ (figure 8) $\epsilon = 1.16$, thus the dipole still has positive net circulation. Finally, when the anticyclonic part becomes stronger (figure 9), $\epsilon = 0.75$. Naturally, the qualitative evolution of the ratio agrees with the observed trajectories. A comparison with the modulated point-vortex model is made using (2.3) and assuming that the dipole was initially symmetric and moved in a southward direction (like the generating cylinder). The initial circulation is $\gamma_0 = \frac{1}{2}(\gamma^+ - \gamma^-)$ as computed at $t = 1.77$ and the experimental $\beta = 0.26$ m^{-1} s^{-1}. A free parameter used to 'tune' the model is L, the radius of the area associated with the point vortices. The values obtained for ϵ, being 1.2, 1.63, 1.14 and 0.74, respectively, compare very well with the corresponding values measured in the experiment (see above). The value of L used to obtain this approximation is 9.44 cm, which is of the same order as

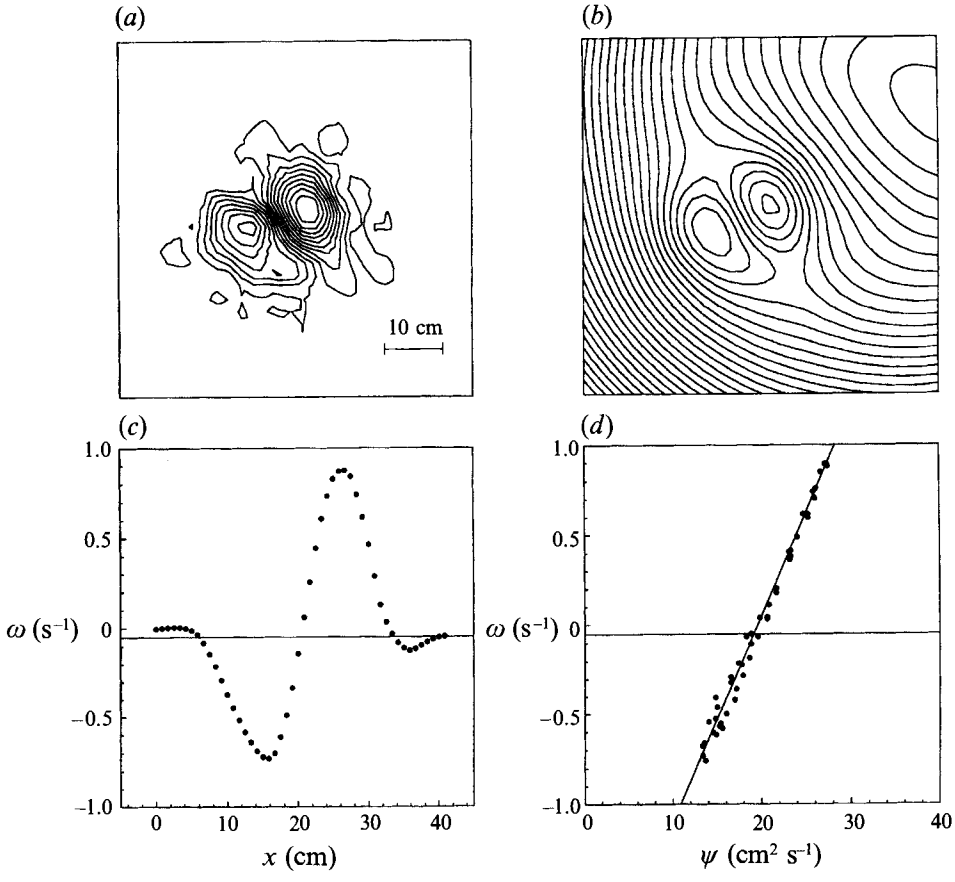

FIGURE 6. Measured flow characteristics of a dipolar vortex on a β-plane at $t = 1.77T$, with $T = 11.3$ s the rotation period of the turntable. The dipole moved initially to the south and subsequently described a meandering path. The graphs represent (*a*) vorticity contours (contour interval 0.1 s^{-1}), (*b*) stream-function contours (contour interval 2 $cm^2\ s^{-1}$) corrected for the observed motion of the dipole, (*c*) distribution of vorticity along a line crossing the points of extremal vorticity values, and (*d*) the ω–ψ relation, obtained by plotting the vorticity value against the stream-function value of every grid point in the interior of the dipole. Experimental parameters: $f = 1.11\ s^{-1}$, $h_0 = 0.17$ m, $s = 0.23\ m^{-1}$, $\beta = 0.26\ m^{-1}\ s^{-1}$.

the distance r between the points of maximal vorticity. Clearly, the condition $L \ll r$, which permits a discrete representation of the vorticity in the point-vortex model, is not satisfied. A smaller L (3 cm) generates values of the ratio ϵ (1.02, 1.05, 1.01 and 0.97, respectively) closer to one than the values measured in the experiment. However, the qualitative evolution of ϵ is the same in the experiments and in the point-vortex model.

A remarkable feature in the vorticity distributions is the presence of a small ring of oppositely signed vorticity around the dipole. The presence of this ring is visible in the form of small humps in the vorticity sections, especially in the first two stages (figures 6*c* and 7*c*). The shielding ring is caused by the advection of ambient fluid in a meridional direction, and its influence on the dynamics of the dipole will be discussed in §5.

A stationary solution of (2.2) satisfies $q = F(\psi)$, where q is the potential vorticity $q = \omega + \beta y$, ψ is the stream function in the system moving with the dipole and F is an arbitrary integrable function. Strictly, in the case of an oscillating dipole a stationary

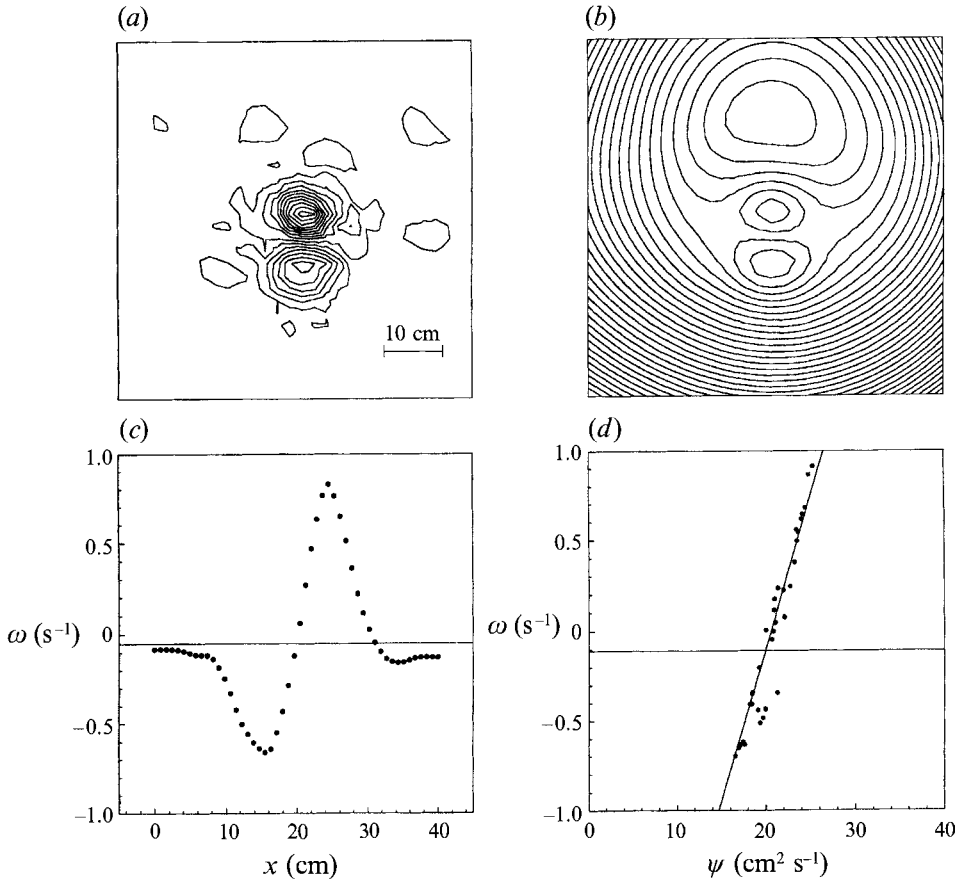

FIGURE 7. As figure 6, but now for $t = 4.42T$.

state is never established: the total circulation oscillates between positive and negative values and the translation velocity changes continuously in direction and in magnitude. In spite of this, values of vorticity and stream function were computed in a frame in which the dipole is 'stationary', by correcting for the instantaneous displacement of the structure.

By plotting the vorticity against the stream function for every node of the interpolation grid, the resultant graph provides information about how close the dipole is to a stationary solution: if the points collapse onto a single line a well-defined functional relationship exists between vorticity and stream function. The scatter around the line can be due to experimental errors but more likely because the structure is not stationary. Furthermore, the form of the curve provides information about the nature of the solution.

The scatter plots presented here are constructed only with points in the interior of the vortex structure; points from the exterior field all collapse onto the horizontal axis ($\omega = 0$). Formally, one should plot the (corrected) potential vorticity $q = \omega + \beta y$, rather than the corrected relative vorticity ω, as a function of ψ. In all experimental results reported here, however, the term βl, with l the radius of the dipole, is at least ten times smaller than ω ($\beta = 0.3$, $l = 0.1$, $0.2 < \omega < 1$), so that ω is a good approximation of q. The difference between scatter plots $\omega(\psi)$ and $q(\psi)$ (not shown here) is in fact hardly noticeable.

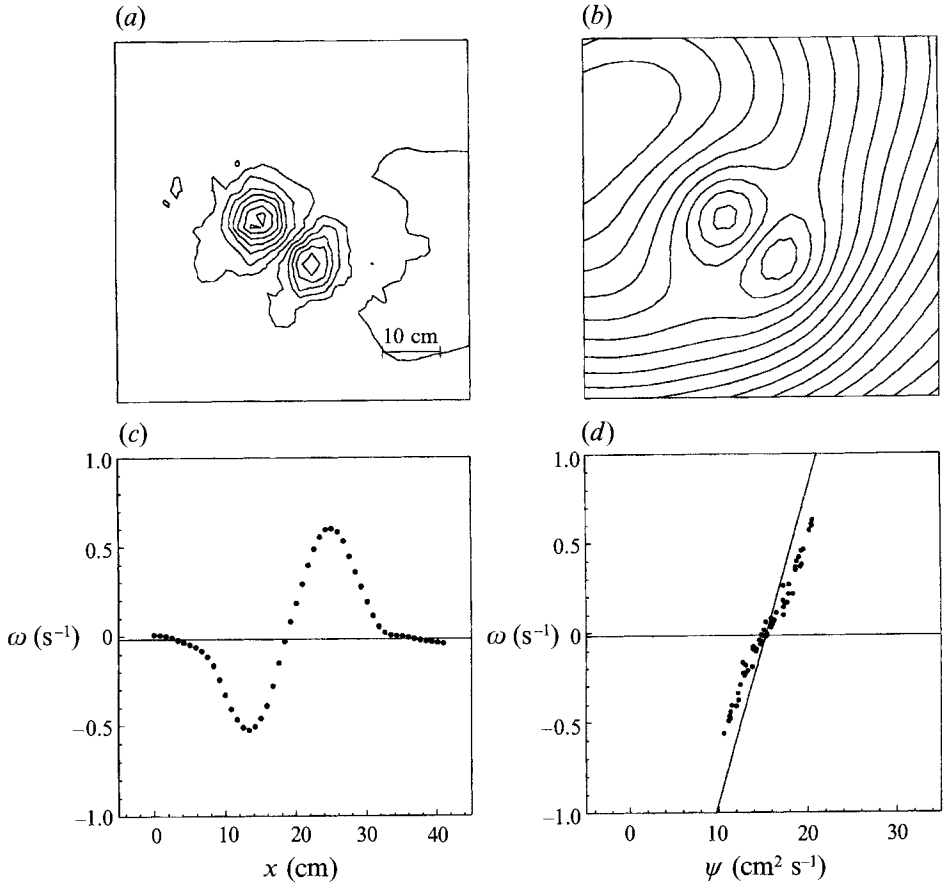

FIGURE 8. As figure 6, but now for $t = 7.96T$.

A linear relation between ω and ψ was observed for the dipole at times $t = 1.77T$ and $4.42T$ (figures 6*d* and 7*d*, respectively). The change in the slope is a consequence of the stretching of the dipole and can be explained as follows. Most analytical dipolar solutions of the equivalent barotropic equation (as well as the Lamb dipole) are based on an assumed linear relation between vorticity and stream function, i.e. $\omega = k^2\psi$ (see Flierl 1987). Under this assumption, the solutions must satisfy the dispersion relation $ka = 3.83$, where a is the radius of the dipole and 3.83 is the first zero of the first-order Bessel function of the first kind, which is one of the building blocks of the modon solutions.

For the laboratory dipoles the radius a is determined by using the closed streamline of the corrected stream-function plot, and then k is calculated using the dispersion relation. This result should agree with the values of k obtained from the scatter plot (the slope is the square of k). Experimental dipoles in the absence of a sloping bottom (f-plane) have been observed to satisfy these criteria. For the experiment being discussed here, it is observed that at $t = 1.77T$ the radius is $a = 11.04$ cm, giving $k = 0.34$. This corresponds very well with the value derived from the scatter plot (figure 6*d*), $k = 0.339$. At $t = 4.42T$, the dipole radius a has decreased to 8.88, giving $k = 0.43$; this value is again in good agreement with the value $k = 0.447$ obtained from the scatter plot (figure 7*d*). At the later stages, $t = 7.96T$ and $15.93T$, a weak nonlinearity in the ω–ψ relation is observed (figure 8*d* and 9*d*). The fitted lines give the

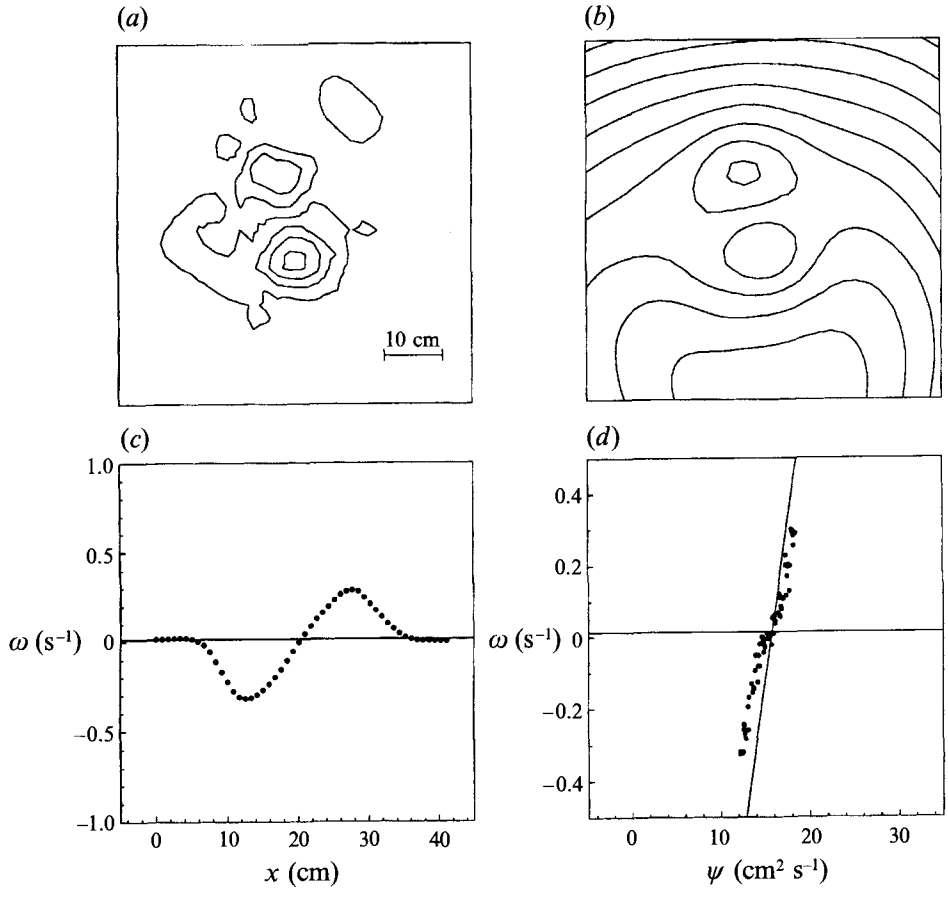

FIGURE 9. As figure 6, but now for $t = 15.93T$.

best approximation of the slope of the two branches. The values of k obtained from the scatter plots are approximately one half of those obtained from the observed radius of the dipole (using the dispersion relation $ka = 3.83$). The disagreement is most likely associated with the nonlinearity of the ω–ψ relation.

4.3. *Trajectory as a function of the tilting angle*

The squeezing and stretching mechanism described at the beginning of this section is active for every initial orientation of the dipole axis. However, its effect is very different on dipoles moving initially at angles greater than $\frac{1}{2}\pi$ (i.e. dipoles with a westward component in their motion) and on dipoles moving at angles smaller than $\frac{1}{2}\pi$ (dipoles with an eastward component).

When its initial angle is less than $\frac{1}{2}\pi$ the dipole acquires an asymmetry of the proper sign to pull it back to its equilibrium latitude. The smooth oscillation of a dipole with initial northeast motion appears in figure 10(*a*), and similar trajectories can be seen in figures 10(*b*) and 10(*f*) for dipoles released in northward and southward directions, respectively. In these three examples the direction of the dipole changes in such a way as to make the structure return to its equilibrium latitude. Because of its own inertia the dipole overshoots and the process repeats.

Dipoles with tilting angles greater than $\frac{1}{2}\pi$ move initially away from the equilibrium

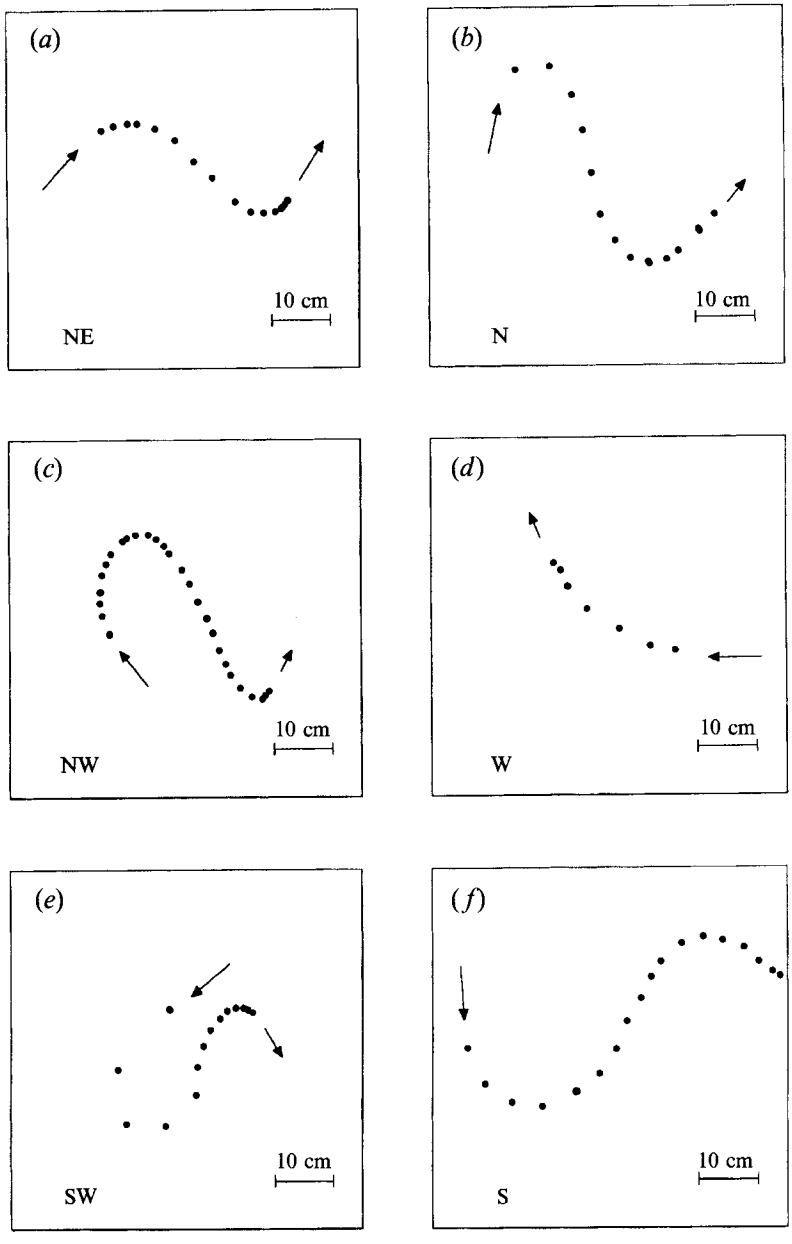

FIGURE 10. Observed dipole trajectories for different initial angles. The dots represent the position of the dipole centre at selected time intervals. Arrows indicate initial and final directions of the observed dipole translation. Since the median depth h_0 of the fluid in the dipole evolution varies from one experiment to another (in the range 15–18 cm) the β-effect changes accordingly in the range 0.25–0.3 $m^{-1}\,s^{-1}$.

latitude before finally returning to it. Figures 10(*c*) and 10(*e*) show examples of initially northwest- and southwest-moving dipoles. Figure 10(*d*) shows the trajectory instability of a dipole shot in a westward direction. In the first two examples the dipoles make looping excursions in a meridional direction before returning to their equilibrium latitude, while in the latter example (cf. figure 10*d*) the dipole breaks up before being able to return to its initial latitude.

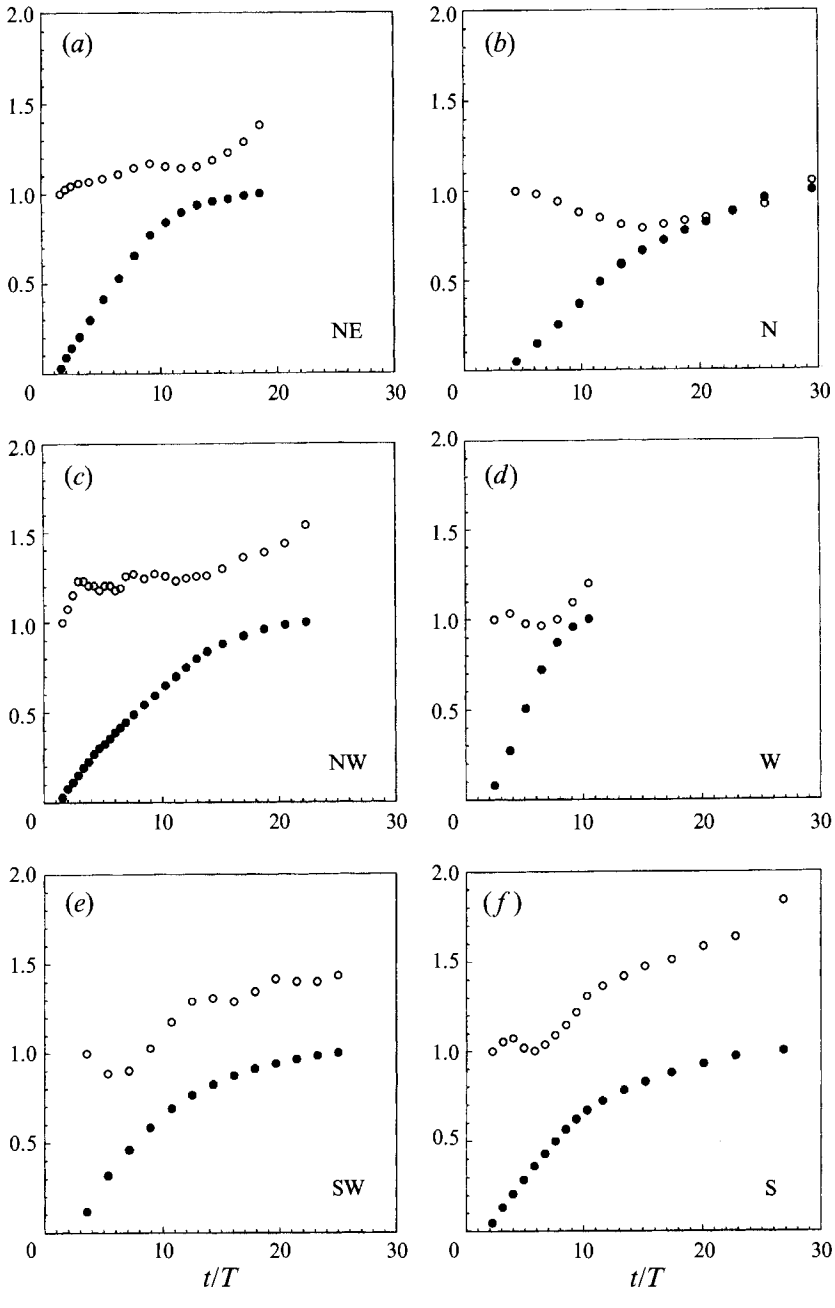

FIGURE 11. Sequence of measured linear displacement (solid dots) and size (open dots) as a function of time (scaled by the rotation period $T = 11.2$ s), for the dipoles shown in the corresponding frames in figure 10. The dipole size is normalized with its size after reaching a mature state (typically 3–4 revolution periods after withdrawal of the generating cylinder). The dipole displacement is normalized with the maximum displacement observed in a particular experiment.

These results confirm numerical and analytical predictions by previous investigations (e.g. Makino *et al.* 1981; Hobson 1991; and Nycander 1992) that an ETD corresponds to a stable equilibrium while a WTD represents the unstable equilibrium.

The evolution of the velocity of the six experiments discussed above can be deduced

from the linear distance travelled by the dipole as a function of time. For the individual experiments of which the observed trajectories are shown in figure 10, the linear displacement of the dipole between successive photographs was measured, and the results (represented by solid dots) are shown in figure 11. A common feature of all cases is that the velocity is approximately constant during the first stages of the evolution, but at later stages it decreases rapidly. Small perturbations can also be observed, which are likely to be produced by two effects. Firstly, the alternating squeezing and stretching of the vortex dipole moving into shallower and deeper areas, respectively, causes oscillations of the velocity magnitude with the same frequency as the meandering motion: the squeezed dipole moves slower than the stretched one. Secondly, the translation velocity of the symmetric dipole is slightly larger than when the vorticity structure is symmetric; this perturbation cycle has a frequency twice that of the meandering cycle. A few attempts were made to extract these perturbation velocities from the data sets shown in figure 11. Although in some cases one can easily observe the cyclic effects described above, most of the results are too noisy to be conclusive.

The alternating squeezing and stretching that the dipole experiences when moving into shallower and deeper areas, respectively, also causes oscillations in the dipole's size. Although the dipole shows a gradual overall increase in size, the oscillatory variations can be clearly recognized in the size measurements for the individual experiments of figure 10, which are represented by the open dots in figure 11. A comparison with the corresponding trajectory plots (figure 10) confirms that the oscillations are the result of displacements in a meridional direction. For example, the southward part of the dipole's trajectory in figure 10(*b*) corresponds with decreasing size (see figure 11*b*), whereas the dipole regains approximately its original size after returning to the initial latitude. In figure 10(*a*) and 11(*a*) one observes a fast growth when the dipole moves northward, followed by a small decrease when it starts to move to the south.

5. WTD versus ETD

An important result from both numerical and analytical calculations of a tilted modon (e.g. Makino *et al.* 1981; Nycander 1992) and its point-vortex counterparts is the dramatic difference between ETD's and WTD's. While dipoles of the former class are stable and perform small oscillations when perturbed, the WTD's are unstable: even an extremely small perturbation causes them to travel over large distances in a meridional direction. This difference was also observed in the laboratory. It was easy to obtain a dipole travelling to the east along an almost straight line. However, we never succeeded in getting a dipole moving to the west in a similar fashion. Very soon these dipoles deviated and drifted a long distance in northern or southern directions before breaking up or colliding with the tank walls (see e.g. figures 10*d* and 10*e*). Note also that in (2.2) steady ETD solutions exist while WTD's always radiate Rossby waves, which were experimentally observed as very weak cells in the wake of the dipole.

A few more differences were observed between eastward- and westward-travelling dipoles. The ETD's were always larger and slower then the WTD's, which were compact and travelled relatively fast. Figure 12(*a*) shows a typical example of the measured size and linear displacement of an ETD: an almost linear growth of the size is clearly observed while the velocity decreases monotonically in a gentle manner. In the evolution of a WTD (figure 12*b*) two stages can be distinguished: in the first stage the dipole experiences a decrease in size and has an almost constant (high) velocity,

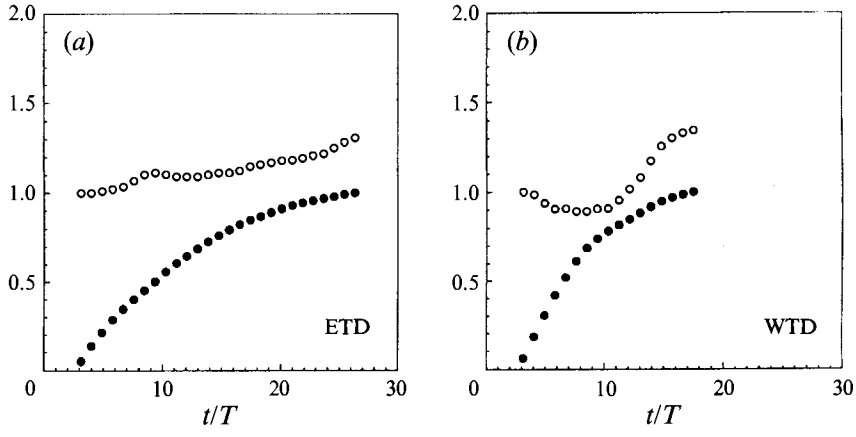

FIGURE 12. Observed dipole displacement and dipole size as in figure 11, but now for: (*a*) an east-travelling dipole (ETD), experimental parameters are $f_0 = 1.12\ \mathrm{s}^{-1}$, $h_0 = 0.17$ m, $s = 0.23\ \mathrm{m}^{-1}$, and $\beta = 0.258\ \mathrm{m}^{-1}\ \mathrm{s}^{-1}$, and (*b*) a west-travelling dipole (WTD), experimental parameters are $f_0 = 1.12\ \mathrm{s}^{-1}$, $h_0 = 0.19$ m, $s = 0.21\ \mathrm{m}^{-1}$, and $\beta = 0.235\ \mathrm{m}^{-1}\ \mathrm{s}^{-1}$.

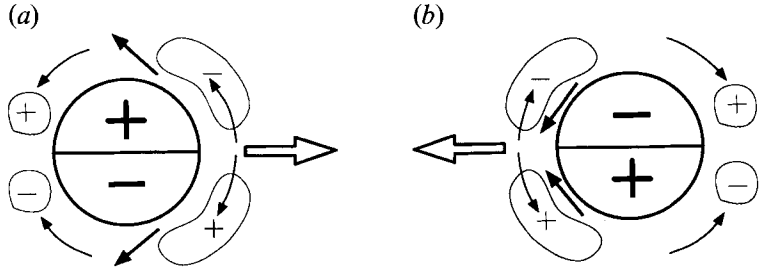

FIGURE 13. Schematic diagram showing the generation of relative vorticity by advection of ambient fluid. The open arrow indicates the translational motion of the dipolar vortex, the thin arrow shows the advection of ambient fluid induced by the moving dipole, and the solid arrow illustrates the tendencies of the dipole halves induced by the secondary vorticity field.

while in the subsequent stage the dipole grows and its drift velocity decreases. This second stage occurs when the dipole has moved to the south as a result of the instability of the westward trajectory. A WTD that drifts to the north shows the same decrease in size (see figures 10*d* and 11*d*) in spite of the squeezing that results from the motion towards shallow water. Pictures of streaklines using exposure times of up to 30 s (not shown here) reveal the presence of weak cells of motion (Rossby waves) in the wake of a WTD, while no clear structure is observed in the wake of an ETD.

The observed differences between ETD's and WTD's can be explained in terms of relative vorticity generation in the fluid exterior to the vortex dipole, due to advection of ambient fluid. If the dipole moves in a zonal direction the sign of the generated vorticity is as follows: in front of the dipole fluid located above the symmetry line moves northward and acquires negative vorticity; on the other hand, below the symmetry line the fluid moves southward and acquires positive vorticity.

Downstream of the dipole the effects are opposite: positive vorticity is generated above the symmetry line and negative vorticity is produced below this line. The schematic diagrams of figure 13 illustrates the process just described for both an ETD and a WTD. According to this mechanism the upstream side of the ETD becomes

'shielded' by patches of opposite relative vorticity, whereas patches of matching vorticity can be expected to be formed in its wake. Besides decreasing the translation speed of the ETD, the secondary vorticity distribution has another important effect: the oppositely signed vorticity shield at the upstream side gives the flow – in combination with the primary vorticity distribution – a double-dipole character that is symmetric with respect to the axis. As indicated by the solid arrows, the upper dipole has a tendency to travel to the north-west, whereas the lower dipole will tend to move to the south-west. In other words the secondary vorticity structure has a tendency (i) to decrease the translation speed, and (ii) to tear the ETD halves apart. In the case of the WTD the advection of ambient fluid results in a band of relative vorticity, as illustrated in figure 13(*b*). In contrast to the ETD, however, the secondary vorticity upstream of the WTD is correlated with the primary vorticity distribution, whereas it is anticorrelated at the downstream side of the WTD. As indicated by the solid arrows, the secondary vorticity structure will most likely tend to enhance the compactness of the WTD and increase its translation speed. These are short-term effects and should be present before a Rossby wave field is established.

In order to verify this conjecture, a numerical simulation using a vortex-in-cell technique was carried out. Except for the modulation of the circulation the method is essentially that described by Christiansen (1973), whose paper should be consulted by readers interested in details of the method. Only the main features are briefly described here: (*a*) the region of interest is divided into a large number of cells and (*b*) each point vortex is supposed to have a finite core so that the (uniform) vorticity in this surface equals the circulation of the point vortex divided by the area.

For every time step the following procedure is carried out:

(i) At the beginning of the time step the position of each particle in the mesh is determined and its *vorticity* is assigned to the four closest mesh points using a bilinear interpolation.

(ii) The vorticity distribution found in step (i) is used as the source term of the Poisson equation (3.4), the solution of which gives the *stream function* in the region.

(iii) The stream function thus found is differenced to give an approximation of the velocity on the mesh points. The *velocity* of each particle is found using the interpolation factors used in step (i). Then each particle is allowed to move with the velocities just calculated for a short time interval.

(iv) Once the new position of each particle is known, its new *circulation* is calculated using (2.3) and the cycle repeats from step (i).

In view of the continuous vorticity distributions observed in the laboratory experiments as discussed in §4.2 (see also figures 6–9), the simulations were initialized by using Lamb's dipole solution. The flow domain was covered by a 33×33 mesh, with periodic boundary conditions at the meridional boundaries, and free-slip conditions at the latitudinal boundaries of the domain. More than 10000 point vortices were evenly distributed over the whole flow domain, although initially only a small number of them (viz. only the ones lying inside the Lamb dipole) have non-zero relative vorticity. The others (lying exterior to the Lamb dipole) are so-called 'ghost vortices' that become active as soon as they are advected in a meridional direction, according to equation (2.3).

The results of the simulations are presented in figure 14. In the following discussion distances are given in units of the initial diameter of the dipole and time in units of the time it takes for the Lamb dipole to travel that unit distance. The graphs on the left (frames *a*, *b* and *c*) show the evolution of the flow field associated with the ETD. At time $t = 0.9$ (figure 14*b*) the dipole has moved a distance of 0.5 units to the east, and

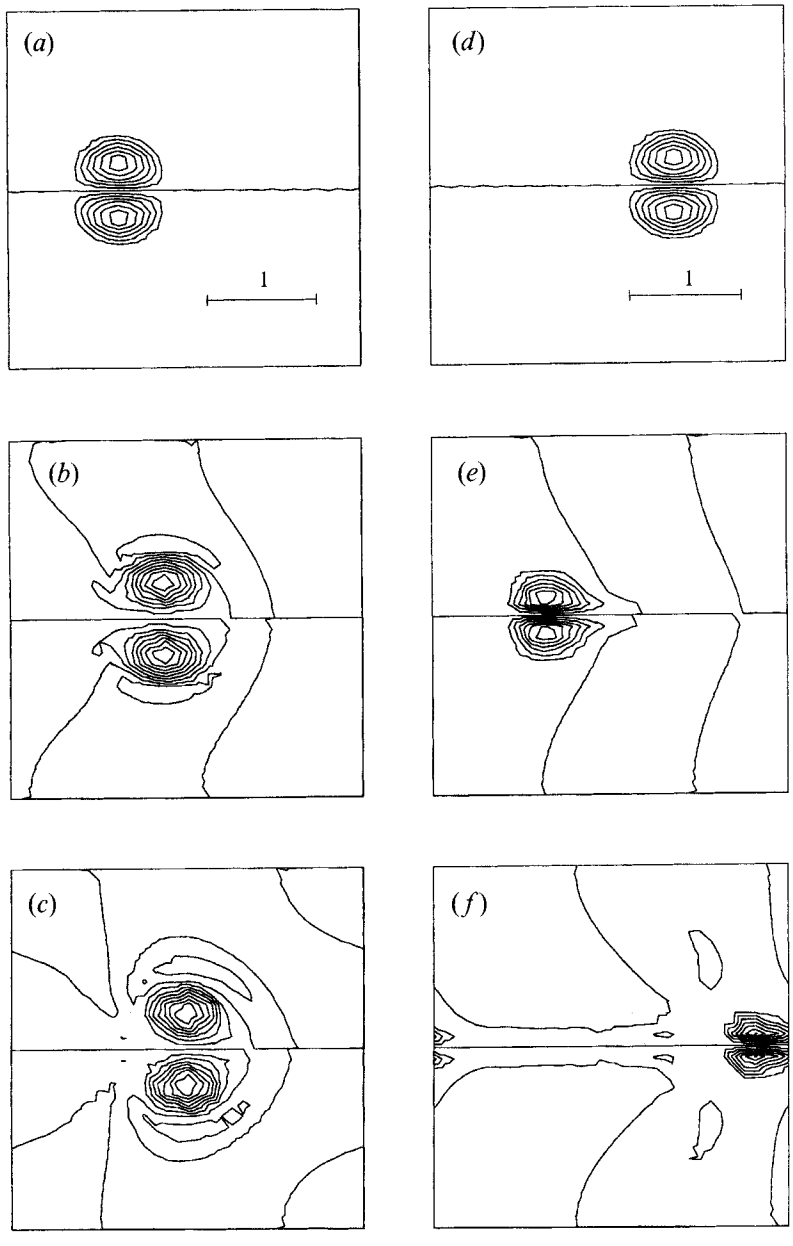

FIGURE 14. Numerical simulations of the evolution of an ETD (*a–c*) and a WTD (*d–f*) using a vortex-in-cell technique. The flow is initialized by taking a Lamb dipolar vortex; boundary conditions are free-slip at the latitudinal walls and periodic in the meridional direction. Vorticity distributions are shown at $t = 0$, $0.9T$ and $1.8T$, where T is here the time required for the Lamb dipole to travel a distance equal to its diameter, in the absence of the β-effect.

has acquired a band of anticorrelated vorticity at its sides; also, one observes the formation of tails at the downstream side, which denote the presence of secondary vorticity, which is correlated with the primary dipole. At $t = 1.8$ (figure 14*c*) the asymmetric structure of the secondary vorticity field is clearly visible. At this stage the ETD has only travelled over a relatively small distance, and shows a considerable widening (in comparison with the initial state shown in figure 14*a*). Although the

simulation was stopped at this stage, the flow behaviour thus found agrees very well with the conjectured ETD behaviour discussed above.

The graphs in the right-hand column of figure 14 (frames *d*, *e* and *f*) show the numerical results for the evolving vorticity distribution associated with the WTD. It is easily observed that the WTD quickly acquires a very compact structure, with tails forming at its downstream side. The compactness of the vorticity structure gives rise to a high translation speed, as can be seen by comparing the WTD graphs with the corresponding graphs of the ETD evolution. At $t = 0.9$ (figure 14*e*) the WTD has shed two patches of oppositely signed relative vorticity, which are the result of the advection of surrounding fluid, as schematically indicated in figure 13(*b*). At $t = 1.8$ (figure 14*f*), the WTD has re-entered the domain at the right (the domain is periodic in the east–west direction), and has become even more compact. All these WTD features confirm the conjectured behaviour outlined above.

6. ETD's for different values of β

The results in the previous section show that the value of β is of primary importance since the magnitude of the secondary vorticity is of order βl, where l is the radius of the dipole. As β is increased the value of the generated vorticity gets closer to the value of the dipole's own vorticity, thus producing a faster growth and eventually a breakup of the dipole. On the other hand, as β decreases, the value of the vorticity generated decreases in comparison with that of the dipole, and for a vanishing β this effect would not be present at all. Indeed, it was observed that on a f-plane the velocity of the dipole remained approximately constant until the dipole reached one of the walls after crossing the tank (figure 15*a*), whereas the size of the structure showed variations but remained very close to its initial value.

For a moderate β value (0.25 m^{-1} s^{-1}) the measured variation of size and velocity of an ETD is shown in figure 12(*a*), while the same quantities are displayed in figure 15(*b*) for a somewhat greater value ($\beta = 0.352$ m^{-1} s^{-1}). Obviously, the qualitative behaviour of the dipole structure is much the same. In the case of a relatively strong β (0.42 m^{-1} s^{-1}) the dipole is observed to split into two monopolar vortices (figure 16*a*). While gradually becoming axisymmetric, these monopolar vortices subsequently start to evolve independently, the cyclonic one (represented by the upper dots) moving to the northwest and the anticyclonic vortex (lower dots) drifting to the southwest, in accordance with the observations reported by Carnevale *et al.* (1991). The evolution of the linear displacement (solid dots) and the distance of the vortex centres (open dots) before, during and after the dipole's breakup is shown graphically in figure 16(*b*). The horizontal part of the curve representing the linear displacement corresponds to the moment when the eastward motion is reversed into a westward one, and can be considered as the point of actual breakup. After the breakup both halves are observed to drift at a similar speed in a westward direction with an additional small meridional velocity component (northward for the cyclonic vortex and southward for the anticyclone).

6.1. *Flow measurements of a splitting ETD*

In order to investigate the dipole splitting process in more detail, an experiment was carried out for a strong β-effect ($\beta = 0.52$ m^{-1} s^{-1}). Again, the initial dipole was directed to the east. The formation of the dipolar structure was completed approximately 4–5 revolution periods after the lifting of the generating cylinder. The spatial distributions of the relative vorticity and the (corrected) stream function of the flow at this stage ($t = 5.27T$) are presented in figure 17(*a*, *b*). In comparison with the

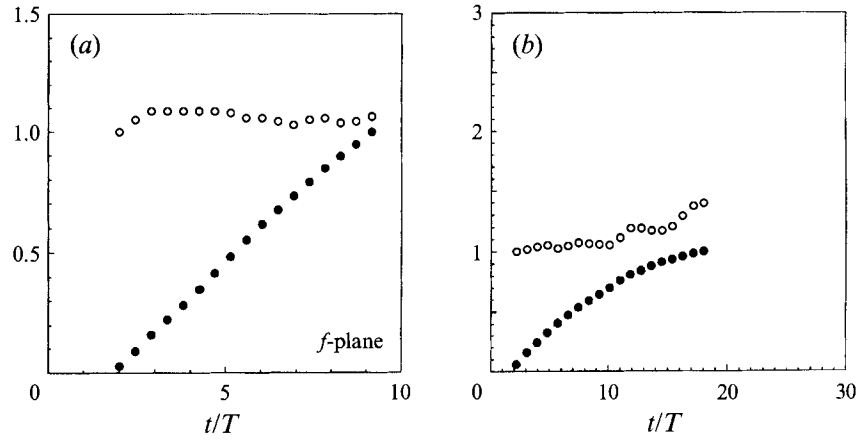

FIGURE 15. Observed dipole displacement and dipole size as in figure 11, but now for (*a*) a dipole on an *f*-plane (experimental parameters $f = 1.12\ \mathrm{s}^{-1}$, $h_0 = 0.2$ m) and (*b*) an ETD on a moderate β-plane ($\beta = 0.352\ \mathrm{m}^{-1}\ \mathrm{s}^{-1}$, $f_0 = 1.1\ \mathrm{s}^{-1}$, $h_0 = 0.17$ m, $s = 0.32\ \mathrm{m}^{-1}$).

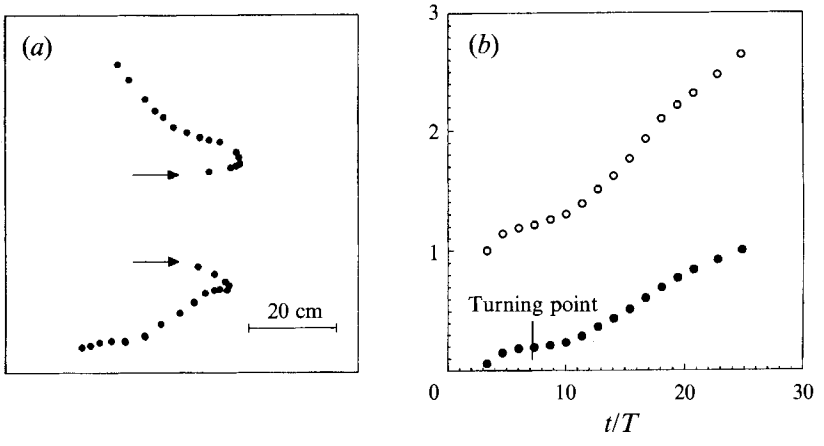

FIGURE 16. Laboratory observations of the breakup of an ETD: (*a*) trajectories of the dipole's vortex centres, the cyclonic half being represented by the upper dots and the anticyclonic half by the lower dots, and (*b*) the linear displacement (solid dots) and the size of the dipole (open dots) as a function of time. Experimental parameters are $f_0 = 1.12\ \mathrm{s}^{-1}$, $h_0 = 0.16$ m, $s = 0.375\ \mathrm{m}^{-1}$, and $\beta = 0.42\ \mathrm{m}^{-1}\ \mathrm{s}^{-1}$.

previously shown dipoles (see figure 6–9), the size of the dipolar vortex is now relatively large, and the two halves are not compactly attached as before. At this stage the structure moved slowly eastward, in a direction perpendicular to the line joining the two vorticity extrema. At a later stage ($t = 14.5T$) the separation between the two halves has clearly increased (figure 18*a*, *b*), and the dipole's breakup was in fact completed. At this point a weak westward drift of the two halves was observed.

The vorticity distribution along the line joining the vortex centres shows that at the earlier stage $t = 5.27T$ (figure 17*c*) the splitting was already in progress: a small kink is clearly visible in the centre of the dipole, which is absent in the weak-β dipoles (see figure 6–9). These observations agree with the numerical results of Couder & Basdevant (1986) who found this result when studying the formation of a vortex couple (in the absence of β-effects) from two initial Gaussian vortices of opposite sign. The corresponding section at time $t = 14.5T$ (figure 18*c*) shows an almost complete breakup of the dipole, and the vorticity distribution resembles that of two isolated

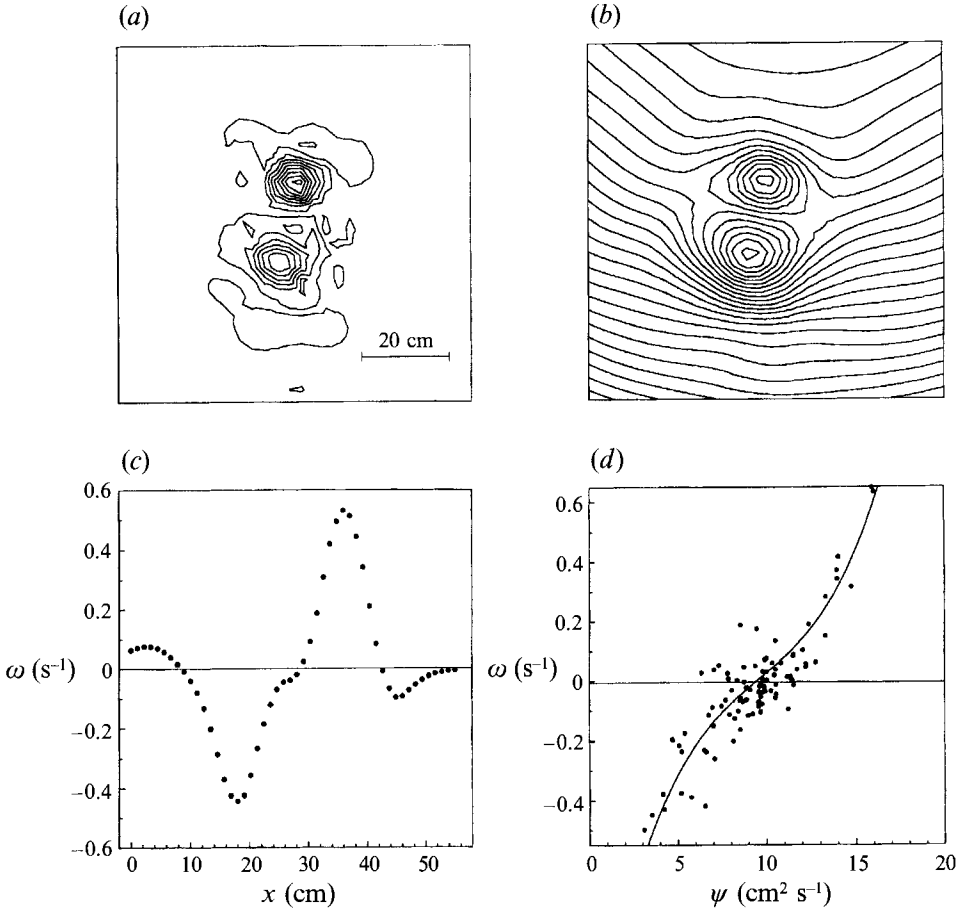

FIGURE 17. Measured flow characteristics of an ETD at an early stage of the splitting process. Time is $t = 5.27T$, with $T = 11.4$ s the rotation period of the turntable: (*a*) vorticity contours (contour interval 0.06 s^{-1}), (*b*) stream-function contours (contour interval 1 $cm^2\ s^{-1}$) corrected for the observed eastward motion of the dipole, (*c*) vorticity distribution along a line intersecting the points of extremal vorticity values, and (*d*) the ω–ψ plot obtained from the grid points in the interior of the dipole. Experimental parameters: $f = 1.1\ s^{-1}$, $h_0 = 0.16$ m, $s = 0.42\ m^{-1}$, $\beta = 0.52\ m^{-1}\ s^{-1}$.

monopolar vortices placed close together. Similar vorticity profiles in single monopolar vortices were measured by Kloosterziel & van Heijst (1992, figures 3*f* and 4*f*).

The ω–ψ plot of the dipole at the former stage (see figure 17*d*) contains considerable scatter (even after corrections), reflecting the non-steadiness of the structure, which was in fact about to undergo the splitting process. However, the points agglomerate around a nonlinear curve. The ω–ψ relation at $t = 14.5T$ (figure 18*d*) shows two antisymmetric branches which are reasonably approximated by a cubic polynomial. Comparison with the ω–ψ relationship of an isolated monopolar vortex, for example as measured by van Heijst, Kloosterziel & Williams (1991, figure 11), confirms that the ω–ψ plot of figure 18*d* indeed represents a combination of a cyclonic and an anticyclonic shielded monopolar vortex. The considerable scatter can be attributed to the different meridional drift components of the vortices (which cannot be simultaneously corrected for), and also to the non-steadiness of the individual vortices: as shown by for example Carnevale *et al.* (1991), the shielded monopolar vortex on a β-plane is not quasi-stationary, and looses vorticity while drifting.

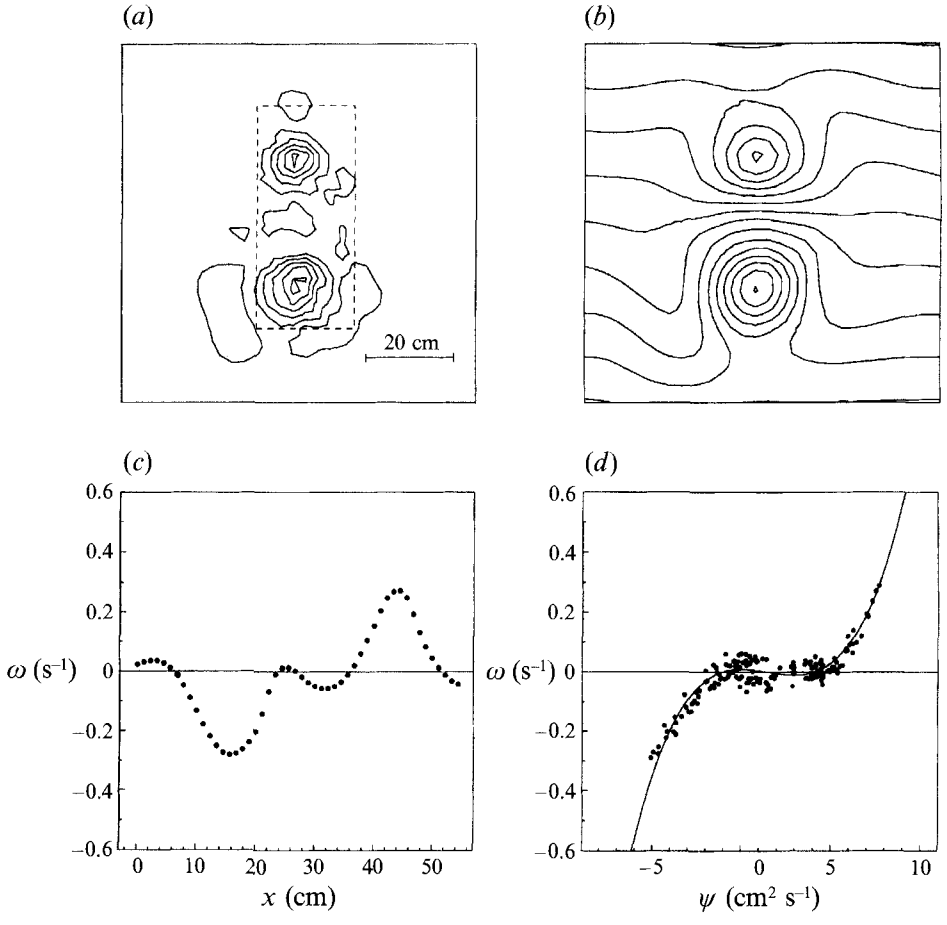

FIGURE 18. Measured flow characteristics of the ETD shown in figure 17 after the splitting has been completed (at time $t = 14.5T$): (*a*) vorticity contours (contour interval 0.06 s^{-1}), (*b*) stream-function contours (contour interval 1 $cm^2\ s^{-1}$) corrected for the observed westward motion of the monopolar vortices, (*c*) vorticity distribution along a line intersecting the points of extremal vorticity, and (*d*) the ω–ψ plot obtained from the grid points in the rectangular area indicated by the broken line in (*a*).

7. Conclusions

According to a point-vortex model vortex couples with the axis tilted with respect of isolines of ambient vorticity will oscillate around these lines. In the linear approximation the amplitude and wavelength of the path grow with increasing initial velocity of the couple and decrease for increasing gradient of ambient vorticity (β). A free parameter in the vortex model is the lengthscale associated with each 'point' vortex. Slightly non-symmetric dipoles will show the same oscillatory behaviour. Strongly non-symmetric couples rotate around a point that moves in a westerly direction.

In a rotating laboratory tank the constant gradient of ambient vorticity is provided by the presence of a sloping bottom. In a series of dye experiments dipoles were initiated at different angles with respect to the isobaths. The trajectories of dipoles with an eastward component in their motion are in good (qualitative) agreement with the results obtained by the point-vortex model and by direct numerical simulations of modons (Kawano & Yamagata 1977; Makino *et al.* 1981). Dipoles with a westward

component agree only in the perturbation enhancement mechanism but do not show the non-translating mode (8-shaped path) or the cycloid-like mode. Only fractions of the looping excursion can be observed. An explanation for this can be found in the large meridional displacements that the non-translating and cycloid-like modes imply. These displacements produce large asymmetries in the dipole leading to strong deformation of the weaker part both by the stronger partner and by the relatively strong advection-generated relative vorticity in the ambient fluid.

Detailed measurements of the velocity field and the vorticity distribution of the dipolar vortex show variations of the total relative circulation as the dipole moves into shallow and deep water, in qualitative agreement with the assumed conservation of potential vorticity. A functional relation is observed between vorticity and stream function, being linear at the first stages and becoming nonlinear at later stages. The slope of the ω–ψ line is observed to increase as the dipole moves into deep water and to decrease when the dipole climbs the topography. This effect is due to variations in the diameter of the vortex structure by alternating stretching and squeezing of the vortex column.

Generation of relative vorticity by advection of ambient fluid in a meridional direction causes ETD's to grow and to translate more slowly, while WTD's become compact and fast-moving during the first stages (before the development of the trajectory instability). The rate of growth of the ETD is determined by the magnitude of the secondary vorticity field, which depends on the gradient of ambient vorticity (β) and the radius of the structure. It is observed that a strong β-effect leads to the breakup of the ETD. After the separation of the dipole into two monopolar vortices, each vortex drifts independently under the β-plane dynamics, namely the cyclonic half moves in a northwestern direction and the anticyclonic vortex travels to the southwest. At an early stage the ω–ψ plot of the ETD is weakly nonlinear (sinh-like), whereas after the breakup the ω–ψ plot has a local maximum and a local minimum, which is typical of two isolated monopoles of opposite sign located close together.

The experimental observations reported here and preliminary numerical results using other topographies (the so-called γ-plane, which simulates the variation of the Coriolis parameter in polar regions or the effect of the parabolic free surface in a rotating fluid) suggest the existence of a general rule of thumb for dipole behaviour, similar to that for monopoles. The new rule would read: dipoles with lengthscales smaller than that of the inhomogeneity will perform oscillations around the corresponding isolines of ambient vorticity, the dipole travelling to the (local) east having a stable trajectory and the dipole travelling to the (local) west an unstable one.

We wish to thank Professor Vyacheslav V. Meleshko for bringing to our attention the work of Love (1944) on the forms of the elastica, and Olaf Gielkens and Elwin van den Bosch for their contribution to the laboratory experiments. We also thank one of the referees for very valuable comments on an earlier version of the paper. One of the authors (O.U.V.F.) gratefully acknowledges financial support from the Dutch Foundation for Fundamental Research on Matter (FOM).

REFERENCES

ADEM, J. 1956 A series solution for the barotropic vorticity equation and its application in the study of atmospheric vortices. *Tellus* **VIII**, 364–372.

BATCHELOR, G. K. 1967 *An Introduction to Fluid Dynamics.* Cambridge University Press.

CARNEVALE, G. F., KLOOSTERZIEL, R. C. & HEIJST, G. J. F. VAN 1991 Propagation of barotropic vortices over topography in a rotating tank. *J. Fluid Mech.* **233**, 119–139.

CARNEVALE, G. F., VALLIS, G. K., PURINI, R. & BRISCOLINI, M. 1988 Propagation of barotropic modons over topography. *Geophys. Astrophys. Fluid Dyn.* **41**, 45–101.

CHRISTIANSEN, J. P. 1973 Numerical simulation of hydrodynamics by the method of point vortices. *J. Comput. Phys.* **13**, 363–379.

COUDER, Y. & BASDEVANT, C. 1986 Experimental and numerical study of vortex couples in two-dimensional flows. *J. Fluid Mech.* **173**, 225–251.

FEDOROV, K. N. & GINSBURG, A. I. 1989 Mushroom-like currents (vortex dipoles): one of the most widespread forms of non-stationary coherent motions in the ocean. In *Mesoscale/Synoptic Coherent Structures in Geophysical Turbulence* (ed. J. C. J. Nihoul & B. M. Jamart), pp. 1–14. Elsevier.

FLIERL, G. R. 1987 Isolated eddy models in geophysics. *Ann. Rev. Fluid Mech.* **19**, 493–530.

FLIERL, G. R., STERN, M. E. & WHITEHEAD, J. A. 1983 The physical significance of modons: laboratory experiments and general integral constraints. *Dyn. Atmos. Oceans* **7**, 233–264.

FLÓR, J. B. & HEIJST, G. J. F. VAN 1993 Experimental study of dipolar vortex structures in a stratified fluid, *J. Fluid Mech.* (Submitted).

HAINES, K. & MARSHALL, J. 1987 Eddy-forced coherent structures as a prototype of atmospheric blocking. *Q. J. R. Met. Soc.* **113**, 681–704.

HEIJST, G. J. F. VAN & FLÓR, J. B. 1989 Dipole formation and collisions in a stratified fluid. *Nature* **340**, 212–215.

HEIJST, G. J. F. VAN, KLOOSTERZIEL, R. C. & WILLIAMS, C. W. M. 1991 Laboratory experiments on the tripolar vortex in a rotating fluid. *J. Fluid Mech.* **225**, 301–331.

HOBSON, D. D. 1991 A point vortex dipole model of an isolated modon. *Phys. Fluids* A **3**, 3027–3033.

KAWANO, J. & YAMAGATA, T. 1977 The behaviour of a vortex pair on the beta plane. *Proc. Oceanogr. Soc. Japan* **36**, 83–84. (In Japanese).

KLOOSTERZIEL, R. C. & HEIJST, G. J. F. VAN 1992 The evolution of stable barotropic vortices in a rotating free-surface fluid. *J. Fluid Mech.* **239**, 607–629.

KONO, M. & HORTON, W. 1991 Point vortex description of drift wave vortices: Dynamics and transport. *Phys. Fluids* B **3**, 3255–3262.

LEGRAS, B., SANTANGELO, P. & BENZI, R. 1988 High-resolution numerical experiments for forced two-dimensional turbulence. *Europhys. Lett.* **5**, 37–42.

LOVE, A. E. H. 1944 *A Treatise on the Mathematical Theory of Elasticity*. Dover (reprinting of the 4th edn., 1927).

MCWILLIAMS, J. C. 1984 The emergence of isolated coherent vortices in turbulent flow. *J. Fluid Mech.* **146**, 21–43.

MAKINO, M., KAMIMURA, T. & TANIUTI, T. 1981 Dynamics of two-dimensional solitary vortices in a low-β plasma with convective motion. *J. Phys. Soc. Japan* **50**, 980–989.

NGUYEN DUC, J. M. & SOMMERIA, J. 1988 Experimental characterization of steady two-dimensional vortex couples. *J. Fluid Mech.* **192**, 175–192.

NYCANDER, J. 1992 Refutation of stability proofs for dipole vortices. *Phys. Fluids* A **4**, 467–476.

NYCANDER, J. & ISICHENKO, M. B. 1990 Motion of dipole vortices in a weakly inhomogeneous medium and related convective transport. *Phys. Fluids* B **2**, 2042–2047.

PEDLOSKY, J. 1979 *Geophysical Fluid Dynamics*. Springer.

READ, P. L., RHINES, P. B. & WHITE, A. A. 1986 Geostrophic scatter diagrams and potential vorticity dynamics. *J. Atmos. Sci.* **43**, 3226–3240.

ROBINSON, A. R. (ED.) 1983 *Eddies in Marine Science*. Springer.

SWATERS, G. E. & FLIERL, G R. 1989 Ekman dissipation of a barotropic modon. In *Mesoscale/Synoptic Coherent Structures in Geophysical Turbulence* (ed. J. C. J. Nihoul & B. M. Jamart), pp. 149–165. Elsevier.

ZABUSKY, N. J. & MCWILLIAMS, J. C. 1982 A modulated point-vortex model for geostrophic, β-plane dynamics. *Phys. Fluids* **25**, 2175–2182.